Robustness of Photonics-based Coherent Multi-Band MIMO Radar to Fiber-based Signal Distribution

A. Malacarne[1], S. Maresca[2], G. Pandey[3], M.M.H. Amir[3], A. Bogoni[3,1], M. Scaffardi[1]

[1]CNIT - Photonic Networks & Technologies National Laboratory (PNTLab), Italy
[2]CNR-IEIIT, Italy
[3]Sant'Anna School of Advanced Studies, TeCIP Institute, Italy
antonio.malacarne@cnit.it

***Abstract* — The impact of radiofrequency (RF) signal distribution through optical fiber links on the performance of a photonics-based coherent multi-band multiple-input multiple-output (MIMO) radar system with widely separated antennas is numerically evaluated. A model of the phase noise induced on each RF band due to fiber transmission among the centralized base station and each radar peripheral (RP), is developed. Numerical Monte Carlo simulations estimating ad-hoc defined key performance indicators (KPIs) identify as main phase noise contributions chromatic dispersion, double Rayleigh scattering (DRS) and mechanical vibrations. In both the two study cases – shipborne and port scenarios – a significant performance worsening occurs for links length of about 20 km.**

***Keywords* — Microwave Photonics, Coherent MIMO Radar, Multi-Band Radar, Phase Noise, Radio-over-Fiber.**

I. Introduction

MIMO radars with widely-separated antennas, thanks to the geometric diversity gain resulting from target observation from various viewpoints, have proved to mitigate the issues of radar cross section (RCS) fluctuations and detection of slow-moving targets [1], ultimately leading to considerable performance for target detection and parameter estimation such as location [1] and velocity [2]. Other diversity domains like frequency diversity can be considered too, with the RPs operating on multiple bands [3]. In addition, if MIMO processing can benefit from a provided phase coherence among all the transmitted and received signals, the resulting resolution can outperform the limit provided by the total interrogated bandwidth, becoming comparable with employed wavelength [1]. Unfortunately, these advantages come at the cost of a high level of system complexity, requiring fine time and phase synchronization among the RPs and long and wideband RF links. However, hybrid microwave photonics (MWP) techniques have emerged as enabling technology addressing both the need for long RF links thanks to optical fiber transmission [4],[5] and the corresponding distribution of multiple coherent bands to an actual radar network thanks to photonics-based up- and down-conversion [6]–[9]. Experimental outdoor demonstrations of MWP-based radar systems [10] including multi-band and widely separated antennas [5] have been realized, together with the identification of the main figures of merit [3],[11].

Here, referring to a photonics-based coherent multi-band MIMO radar architecture, the modeling of the phase noise originating from the distribution of RF signals through optical fiber links has been defined. Its impact has been analyzed through relevant KPIs that have been estimated in two use cases, i.e. shipborne scenario (fiber links length of hundreds of meters) and port scenario (fibre links length of few kilometers).

II. System Architecture

The reference architecture of the proposed photonics-based coherent multi-band MIMO radar system is depicted in Fig. 1.

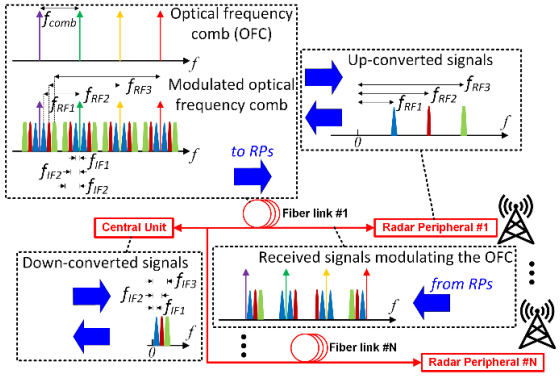

Fig. 1. Schematic of the photonics-based coherent multi-band MIMO radar system showing signal distribution among central unit and radar peripherals through optical fiber links.

In a central unit multiple (three in this case) radar signals – e.g. frequency-modulated continuous waves (linear chirp) – are generated, each at a distinct intermediate frequency (IF): f_{IF1}, f_{IF2} and f_{IF3} in this example. In parallel, an optical frequency comb (OFC) with mode spacing f_{comb} is obtained for instance through opto-electronic modulation driven by an electric local oscillator at frequency f_{comb}. The OFC is then modulated through an opto-electronic Mach-Zehnder modulator (MZM) driven by the sum of the intermediate-frequency radar signals. Both the modulated OFC and its unmodulated version are sent through optical fiber links to multiple RPs. Each RP is able to both transmit and receive the signals at each RF band, through suitable front ends. The strategy to distinguish, for each received echo, the corresponding RP transmitter, is time division multiplexing (TDM). At each RP the modulated and unmodulated OFC get separated (e.g. via spatial separation with distinct fibers, exploiting polarization diversity, wavelength diversity) and the modulated version enters a photodetector (PD) to generate, at its output, the up-converted multi-band radar signal. In

particular, each f_{IF} gets up-converted to a distinct f_{RF} as exposed in the example reported by Fig. 1. The unmodulated version of the OFC is modulated, once again through an opto-electronic MZM, driven by the back-reflected echoes. Such modulated OFC version is sent back through the fiber link to the central unit, where another PD (one for each RP) generates multiple beating terms, including those at the original intermediate frequencies. Such down-converted signals are digitized and processed in a centralized and coherent fashion.

III. Modelling of the Phase Noise due to Signal Distribution through Optical Fiber

To guarantee the superior performance provided by the coherent MIMO processing strategy, the degree of phase coherence among the received echo signals is crucial and, in the architecture shown in Fig. 1, this might be significantly affected by various sources of phase noise taking place during optical fiber transmission of the signals, which are listed here below.

A. Thermodynamic fluctuations

The thermodynamic fluctuations induce a fluctuation of the refractive index and physical length of the fiber. This causes group delay variations which lead to phase noise (PN) [12]. The power spectral density (PSD) of such PN term on each generated RF carrier (and signal) is derived in [13] and is proportional to the fiber length L and to the square of the generated radiofrequency f_{RF}.

B. Amplitude-to-phase noise conversion

Another PN term origins from amplitude-to-phase modulation (AM-PM) conversion in the PD or in other microwave components [14]. The PN is induced by the optical relative intensity noise (RIN) – including RIN occurring in the laser – as well as RIN induced by processes within the optical fiber, such as DRS. The relation between the single-sideband PN due to AM-PM conversion and the PSD of the RIN is expressed as [12]:

$$\mathcal{L}_{AM-PM} = \frac{1}{2}\left(\frac{d\phi}{dP/P}\right)^2 S_{RIN}(\omega) \qquad (1)$$

where $d\phi/dP$ is the derivative of the microwave phase to the optical power P and $S_{RIN}(\omega)$ is the PSD of the laser RIN. Consequently, the AM-PM conversion-induced microwave PN has no explicit dependence on L and f_{RF}.

C. Chromatic dispersion

The group velocity of light propagating along the fiber depends on its optical frequency because of the chromatic dispersion. Hence, the signal group delay in fiber varies due to the frequency noise of the laser and will induce microwave PN [15]. Such PN term can be expressed as [12]

$$\mathcal{L}_{CD}(\omega) = \frac{1}{2}\left(\frac{\omega_{RF}\lambda^2 D_\lambda}{c}\right)^2 L^2 S_{\vartheta,laser}(\omega) \qquad (2)$$

where λ is the laser wavelength, D_λ is the dispersion coefficient of the optical fiber, $S_{\vartheta,laser}(\omega)$ is the PSD of the laser frequency noise, and $S_{\vartheta,laser}(f) = f^2 \times S_{\phi,L}(f)$ where $S_{\phi,L}(f)$ is the PSD of the laser PN. Hence, the chromatic dispersion-induced microwave PN is directly proportional to the square of L and to the square of $\omega_{RF} = 2\pi f_{RF}$.

D. Double Rayleigh scattering

Microscopic variations of the material density along the fiber cause Rayleigh scattering, i.e. a portion of light scatters at an angle of ~180^0 with respect to the original propagation direction, thus traveling in the opposite direction to that of the incident light. Again, a portion of the once-reflected light is reflected back and travels in the direction of the initial incident light but with a delay equal to the path between the two scattering points. The double scattered light and the original incident light interfere with each other, modulating the intensity of the light. This process causes optical RIN which induces microwave PN [16]. The DRS-induced microwave PN grows super-linearly below a certain fiber length over certain ranges of offset frequency and above that value, the PN grows linearly or sub-linearly. The magnitude of the laser PN determines the transition between these two regions [17]. The DRS-induced microwave PN is independent of microwave frequency. An analytical expression can be found in [16]. Higher order Rayleigh scattering has not been considered as it has negligible impact on system performance.

In [12], where the different noise contributions have been calculated as a function of the frequency offset with respect to f_{RF} and for a quiet fiber installed underground (no mechanical vibrations), it comes out that the main contributions to PN are given by double Rayleigh scattering and chromatic dispersion, with the rest of phenomena that are negligible.

The estimated total PN PSD due to transmission over a certain fiber length L for a specific microwave frequency f_{RF} is,

$$\mathcal{L}(L, f_{RF}) = 10 \times log_{10}(PN \cdot L^2 \cdot f_{RF}^2) \text{ [dBc/Hz]} \qquad (3)$$

where PN is the PN PSD per fiber length unit and frequency unit, extrapolated from the experimental curves in [12]. Eq. (3) represents an overestimation, as here the PN PSD scales with the square of both L and f_{RF} whereas the DRS, as previously explained, only scales with L.

E. Mechanical vibrations

For scenarios with the optical fibers for radar signals distribution deployed into terrestrial, maritime or air vehicles, where the engines vibrations and the oscillations induced by rough terrain, sea waves and air turbulence respectively, are relevant, mechanical vibrations contribute at low frequency offsets, i.e. from 1 Hz to 10 kHz. These fiber vibrations cause phase fluctuations in the transmitted signal propagating through the fiber. These fiber vibration-induced phase fluctuations are relevant in shipborne coherent MIMO radars and may affect the KPIs of the designed MIMO radar system. Vibrations are commonly measured as acceleration [18]. The bound between the mechanical vibrations and their impact on the microwave signal PN is expressed in [19], where the vibration impact on different type of fiber is analyzed. We have extrapolated the results of [19] to analyze the effect of

the vibrations in the engine and machinery of a vessel on the phase fluctuations of the transmitted signal through the fiber in a shipborne coherent multiband MIMO radar. In [19], peak acceleration was 13.84 m/s^2. This analysis considers the relevant accelerations for an actual vessel scenario (40 m/s^2) [18] and extrapolates the resulting phase noise based on these accelerations. Assuming a linear dependence between the PN PSD and peak acceleration, for a reference $f_{RF} = 10\ GHz$ and single-mode fiber (SMF) length $L = 1\ km$, the total extrapolated PN PSD for a vessel is shown in Fig. 2 where the impact of vibrations is evident from 1 Hz to 10 kHz and at higher detuning frequencies DRS and chromatic dispersion effects are also highlighted. For detuning higher than 1 MHz a typical Flicker noise decay is assumed.

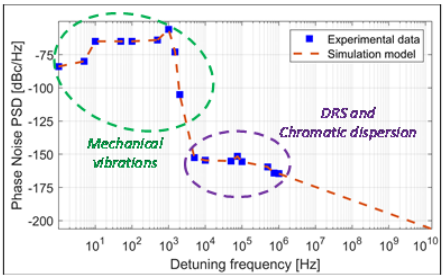

Fig. 2. Extrapolated PN PSD when vibrations effects are taken into account (Curve obtained for f_{RF} = 10 GHz, 1 km SMF).

IV. Photonic-based MIMO radar robustness evaluation

KPIs related to the ambiguity function were evaluated for a coherent multi-band MIMO radar system using MATLAB simulations. Two scenarios, shipborne and port, were considered. In the latter case vibrations similar to the shipborne case and the effect of heavy vessel traffic have been considered.

A. Shipborne scenario

In the shipborne scenario, the RPs are widely separated along a 100-m long linear baseline and consist of 2 transmitters and 4 receivers (TX coordinates -50m, +25m, RX coordinates -25m, -10m, +10m, +50m), each working at three RF bands (9/10/11 GHz) 600 MHz-wide each, for a total of 24 virtual channels. PN between different bands and the Tx/Rx components are mutually independent in our consideration. The strategy to distinguish the transmitter is TDM. Each radar signal from/to the base station to/from each RP is assumed to be delivered through SMF and the impact of different fiber lengths has been analyzed. The evaluated KPIs for a point-like scatterer at a distance of 1200 m are range resolution, cross-range resolution, peak-to-average sidelobe ratio (PASR), peak-to-maximum sidelobe ratio (PMSR), and target localization accuracy.

Since the PN model involves very low detuning frequencies, a long pulse train has been simulated to achieve an integration time in the millisecond regime. In this case 100 ns-long pulses are simulated with a 10 µs pulse repetition interval. 1000 pulses are then generated, to achieve a total pulse train time duration of 10 ms. Realistic additive white Gaussian noise and SNR evolution are considered on each received signal. The first takes into account SNR of the generated signals and receiver noise, whereas the latter scales with the received signal power that depends on the target distance. For each considered fiber length, both the mean value of the calculated parameter and its distribution variance are shown for a Monte Carlo simulation. Looking at Fig. 3, it can be observed that significant worsening in terms of range and cross-range resolution occurs for fiber lengths larger than 25 km. Similarly, a correct localization of the target is achieved up to a fiber length of 25 km. On the other hand, PASR and PMSR significantly decrease for fiber lengths larger than 10 km and 20 km respectively. Since the considered scenario is a shipborne one, a maximum of a few hundred meters of fiber per link is enough to connect the base station to each RP. For this reason, the conclusion in this case is that the use of fiber links preserves a level of coherence absolutely sufficient to enable correct coherent MIMO processing.

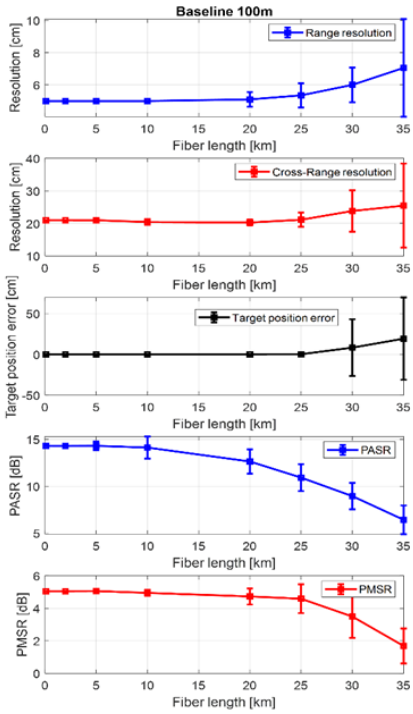

Fig. 3. Evolution of the main KPIs of a tri-band 2×4 MIMO radar with 100-m baseline and RF frequencies 8, 9 and 10 GHz, in presence of optical fiber transmission-induced PN, for varying the fiber length and in a Monte Carlo simulation. For each Monte Carlo simulation both the mean value of the calculated parameter and its distribution variance are shown.

B. Port scenario

In a second example, a linear baseline as long as 1 km is considered, similarly to a port scenario. The antenna locations are simply scaled up with respect to the previous case. By comparing Fig. 4 (blue curves) with Fig. 3, it is confirmed that even with a longer baseline and changing the target distance (2500 m here), the trend of each KPI is basically the same. This means that the optical fiber transmission of RF signals is not a problem even in the port scenario, as long as the base station is not at a distance greater than 20 km from the radar

peripherals. A set of higher frequencies, i.e. 10/11/12 GHz has been tested as shown by Fig. 4 (red curves). A more pronounced worsening behavior for higher frequencies is notable concerning target localization and both PASR and PMSR. Such a trend is not straightforward when comparing range resolution and cross-range resolution, as the coherent MIMO data fusion process leads to a resolution related to the employed wavelengths that, for higher frequencies, are lower. Fig. 5 shows the excellent resolution provided by coherent MIMO processing with 5km-long fiber links and its malfunction with 35km-long links.

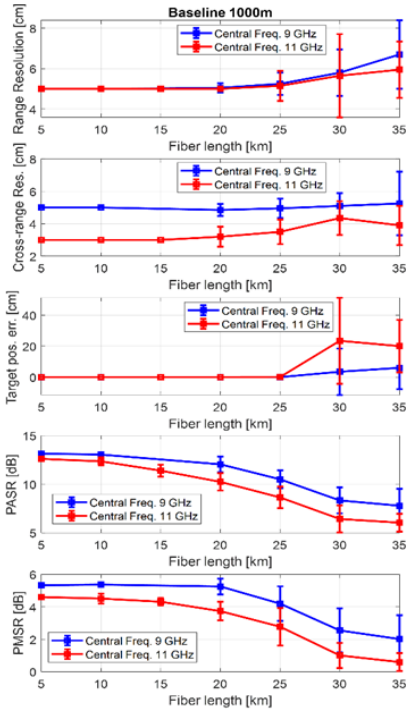

Fig. 4. KPIs for a 1000-m baseline and RF frequencies 8/9/10 GHz and 10/11/12 GHz.

V. Conclusion

The potential performance of a photonics-based coherent multi-band MIMO radar system considering RF signal distribution among the centralized base station and each radar peripheral through optical fiber links, have been evaluated through Monte Carlo simulations. A model of the phase noise induced on each RF band due to fiber transmission has been developed. In the two considered use cases, i.e. MIMO radar located on a ship and in a port, the impact on the performance has been verified to be negligible unless the base station is located at an average distance ≥ 20 km from the peripherals.

Acknowledgment

This work was partly funded within the project COSMOS by the FISR funding scheme, Italian Ministry of University and Research, grant number FISR2019_03476, and by the "EU under the Italian National Recovery and Resilience Plan (NRRP) of NextGenerationEU, partnership on "Telecommunications of the Future" (PE00000001 - program "RESTART").

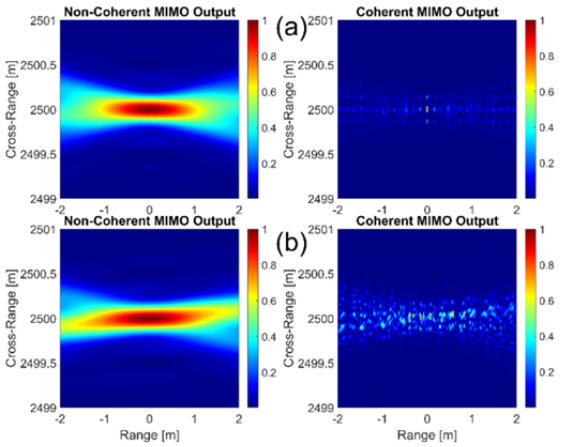

Fig. 5. Non-coherent and coherent MIMO ambiguity function for 10/11/12 GHz carrier frequencies and 5 km-long (a) and 35 km-long (b) fiber links.

References

[1] A. M. Haimovich, et al., "MIMO Radar with Widely Separated Antennas," IEEE Sig. Proc. Mag., vol. 25, no. 1, pp. 116-129, 2008.

[2] Q. He, et al., "Target velocity estimation and antenna placement for MIMO radar with widely separated antennas", IEEE J. Sel. Top. Signal Process., vol. 4, no. 1, pp. 79-100, Feb. 2010.

[3] S. Maresca, et al., "Information Diversity in Coherent MIMO Radars," 2021 IEEE Radar Conference, Atlanta, GA, USA, 2021, pp. 1-6.

[4] A. Malacarne, et al., "Coherent Dual-Band Radar-Over-Fiber Network With VCSEL-Based Signal Distribution," IEEE J. of Light. Tech., vol. 38, no. 22, pp. 6257-6264, Nov., 2020.

[5] S. Maresca, et al., "Field Trial of a Coherent, Widely Distributed, Dual-Band Photonics-Based MIMO Radar With ISAR Imaging Capabilities," IEEE J. of Light. Tech., vol. 40, no. 20, pp. 6626-6635, Oct., 2022.

[6] J. Capmany, D. Novak, "Microwave photonics combines two worlds", Nature Photonics, vol. 1, pp. 319-330, 2007.

[7] J. McKinney, "Photonics illuminates the future of radar", Nature, vol. 507, pp. 310-312, 2014.

[8] A. Bogoni, P. Ghelfi and F. Laghezza, Photonics for Radar Networks and Electronic Warfare Systems, London:IET SciTech Pub., 2019.

[9] G. Serafino, et al., "Microwave Photonics for Remote Sensing: From Basic Concepts to High-Level Functionalities", IEEE J. of Light. Tech., vol. 38, no. 19, pp. 5339-5355, Oct. 2020.

[10] G. Serafino et al., "Maritime Field Trial of a Dual-Band Silicon Integrated Photonics-Based Radar," IEEE J. Sel. Top. Quantum Electron., vol. 28, no. 5, pp. 1-10, Sept.-Oct. 2022.

[11] G. Serafino, et al., "Key Performance Indicators for System Analysis of MIMO Radars with Widely Separated Antennas," 19th European Radar Conference (EuRAD), Milan, Italy, 2022.

[12] J.P. Cahill *et al.*, "Additive phase noise of fiber-optic links used in photonic microwave-generation systems," Appl.Opt. 56, B18-B25, 2017.

[13] L. Duan, "General treatment of the thermal noises in optical fibers," Phys. Rev. A 86, 023817, 2012.

[14] J. Taylor *et al.*, "Characterization of power-to-phase conversion in high-speed P-I-N photodiodes," IEEE Photon. J. 3, 140–151, 2011.

[15] K. Volyanskiy *et al.*, "Contribution of laser frequency and power fluctuations to the microwave phase noise of optoelectronic oscillators," J. Lightwave Technol. 28, 2730–2735, 2010.

[16] P. Wan and J. Conradi, "Impact of double Rayleigh backscatter noise on digital and analog fiber systems" J. Lightw. Technol. 14, 288–297, 1996.

[17] J. P. Cahill *et al.*, "Superlinear growth of Rayleigh scattering-induced intensity noise in single-mode fibers," Opt.Express 23, 6400–6407, 2015.

[18] https://www.cdinfo.lr.org/information/Documents/LRGuidance/Vibration%20&%20Noise%20Guidance%20Notes%202.pdf

[19] J. Taylor et. al, "Vibration-induced PM noise measurements of a rigid optical fiber spool," 2008 IEEE International Frequency Control Symposium, 2008, pp. 807-810, doi: 10.1109/FREQ.2008.4623110.